powders

MDPI

Article

Mechanical, Corrosion, and Ion Release Studies of Ti-34Nb-6Sn Alloy with Comparable to the Bone Elastic Modulus by Powder Metallurgy Method

Mariana Correa-Rossi [1,2,*], Liliana Romero-Resendiz [3], Daniel Leal-Bayerlein [4,5], Ana Liz Garcia-Alves [1], Francisco Segovia-López [2] and Vicente Amigó-Borrás [2]

1 Cell Therapy and Regenerative Medicine Lab, Department of Veterinary Surgery and Animal Reproduction, School of Veterinary Medicine and Animal Science, Sao Paulo State University, UNESP, Botucatu 18618-681, SP, Brazil; ana.liz@unesp.br
2 Institut de Tecnologia de Materials, Universitat Politècnica de València, Camí de Vera s/n, 46022 Valencia, Spain; fsegovia@mcm.upv.es (F.S.-L.); vamigo@upv.edu.es (V.A.-B.)
3 Metallic and Ceramic Materials Department, Instituto de Investigaciones en Materiales, Universidad Nacional Autónoma de México, Circuito Exterior S/N, Cd. Universitaria, A. P. 70-360, Coyoacán, Mexico City 04510, Mexico; liliana.rom7@comunidad.unam.mx
4 Materials Science and Technology Center, Nuclear and Energy Research Institute (IPEN), Sao Paulo 05508-000, SP, Brazil; danielbayerlein@icloud.com
5 Technological Research Institute (IPT), Sao Paulo 05508-901, SP, Brazil
* Correspondence: mariana.rossi@unesp.br

Abstract: The development of a Ti-34Nb-6Sn alloy by the powder metallurgy method, employing two different compaction conditions, A (100 MPa) and B (200 MPa), was carried out. To evaluate the feasibility of the Ti-34Nb-6Sn alloy as an implant biomaterial, microstructural and mechanical characterizations, as well as corrosion susceptibility and ion release tests, were performed. Results indicated microstructures dominated by the presence of β-Ti phase and a lower percentage of α-Ti and Nb phases. The porosity percentage decreased when the compaction pressure increased. Both conditions presented a good match between the elastic moduli of the alloy (14.0 to 18.8 GPa) and that reported for the bone tissue. The Ti, Nb and Sn ions released for both compaction conditions were within the acceptable ranges for the human body. Condition B showed higher corrosion resistance in comparison with condition A. Based on the obtained results, the produced porous Ti-34Nb-6Sn alloys are feasible materials for orthopedic implant applications.

Keywords: elastic modulus; ion release; corrosion; mechanical behavior; biomaterial

check for updates

Citation: Correa-Rossi, M.; Romero-Resendiz, L.; Leal-Bayerlein, D.; Garcia-Alves, A.L.; Segovia-López, F.; Amigó-Borrás, V. Mechanical, Corrosion, and Ion Release Studies of Ti-34Nb-6Sn Alloy with Comparable to the Bone Elastic Modulus by Powder Metallurgy Method. *Powders* **2022**, *1*, 3–17. https://doi.org/10.3390/powders1010002

Academic Editor: Jai-Sung Lee

Received: 26 September 2021
Accepted: 17 January 2022
Published: 25 January 2022

1. Introduction

The increase in population life expectancy and the decline in birth rates have increased the need for the use of orthopedic implants [1,2]. By 2009, it was estimated that musculoskeletal disorders cost around USD 254 billion [2]. In addition, it is forecast that by 2030, the number of hip replacements and total knee arthroplasties will increase by 174% and 673%, respectively, from the 2009 rate. In orthopedic repairing, the devices used most often are based on metallic, ceramic and polymer materials [3], as they can almost recover the full function of bone tissue for a significant duration [4]. Among the metallic devices, the most commonly used metals are stainless steel, Co-Cr alloy, titanium (Ti) and Ti alloys, such as Ti-6Al-4V [5]. Titanium has promising characteristics for biomaterials, such as high mechanical strength, medium elastic modulus, low susceptibility to corrosion and good biocompatibility [6,7]. For these reasons, more than 70% of the devices used have Ti in their composition [8,9]. The most widely used Ti alloy (Ti-6Al-4V) includes aluminum and vanadium, components that are known as cytotoxic and which can lead to neurological

and respiratory disorders [10,11]. Therefore, searching for new components that can be used for long periods without damage to human health is an essential task.

Metal ions that are released from these biomaterials can be transported by body fluids, accumulate in the organs and promote allergenic and carcinogenic effects [9]. According to some authors, the concentrations of chloride ions (Cl^-) in the serum and the interstitial fluid are in the range of 113–117 mEq L^{-1}. Thus, this environment can lead to the corrosion process of metallic biomaterials when in contact with such bio-fluids. Besides, the body fluid is composed of proteins (electrolytes) that can also ignite the corrosive process [12,13]. In addition, the oxygen content that is present in the body fluid is 25% of that in the atmosphere [14]. This low oxygen content can delay the formation of protective oxide layers on the surface of the implants. As a result, a significant amount of metal ions are released into the body fluid. In the natural condition, the pH of the body fluid is kept practically constant, due to its ionic composition of buffering character. Normally, the pH value is in the range of 7.0 to 7.35 [15]. However, when a patient is exposed to orthopedic surgery, the pH of the fluid around the bone tissue changes, decreasing to approximately 5.2. After a few weeks, the natural conditions are restored, returning to the range of 7.0–7.35 [15]. However, even with the buffering character of the body fluid, the pH value can change depending on several factors, such as the dissociation of proteins and the type of cells present. This could influence the corrosion of metallic implants. As they are non-toxic, niobium (Nb) and tin (Sn) are good candidates for Ti alloy-based biomaterials, also combining good stiffness and osseointegration response [16–18]. The non-toxicity of Nb and Sn is extremely important, as these materials will be in contact with body fluids, which can stimulate the process of ions' release into the bloodstream. As a consequence, new Ti-based alloys with non-toxic elements such as Zr, Nb, Ta and Sn were developed [6]. Ti-Nb-based alloys that contain non-toxic elements have attracted extensive fundamental research attention due to their low elastic modulus and shape memory behaviors, as well as their super-elasticity [7]. The corresponding alloying elements stabilized the titanium BCC crystal structure at room temperature and hence decreased the elastic modulus [8]. Metastable β Ti alloys are found in the Ti-Nb system when the amount of β stabilizer is sufficient to avoid α martensitic formation during cooling. Nb can dissolve perfectly in Ti and exists in solid solution [9,13]. The element acts as a β-stabilizing element in Ti Alloys. Meanwhile, the second-phase α martensitic formation, which has a hexagonal crystal structure, tends to increase hardness and embrittle the alloy [10]. Therefore, it is important to control the content of α phase. Sn is a potential alloying element for use in preventing the excessive α phase precipitation in β phase. [19–22]. Both Nb and Sn are non-cytotoxic because they have little effect on mouse fibroblast-derived L929 cells and mouse osteogenic MC3T3-E1 cells [23], and the non-cytotoxicity of Ti-Nb-Sn alloys has been reported in the literature [24–26].

Concerning the manufacture of alloys, there are two classic routes in powder metallurgy. The first one is by pre-bonding (PA) and the second one is using the elemental mixture. The combination of a sintering route and conventional uniaxial compaction of the powders obtained by elemental mixing is an economical process for obtaining Ti alloys. Additionally, this combination is fast to perform and requires temperatures lower than the melting point of the alloying elements. Parameters such as compaction pressure, sintering temperature, speed and milling time of powders have a strong influence on the final microstructure and properties of the alloy. Furthermore, powder metallurgy offers the possibility of modifying the porosity of the piece, providing an elastic modulus value close to that of bone, especially when compared to the cortical bone [27]. The powder metallurgy allows to very economically obtain porosities of 20–25% while still maintaining the mechanical properties at sufficiently high rates. A porosity between 20% and 50% can promote better cell–tissue–prosthesis interactions [19]. However, the limitation of this technique regards the part that is difficult to remove from the matrix [27,28]. Due to these difficulties, it is possible to resort to more advanced or special techniques, such as cold isostatic pressing (CIP) or hot isostatic pressing (HIP), and in recent years to additive

manufacture fabrication, but these are higher-cost techniques than the conventional press and sinter. However, the difficulties in producing near-net-shapes by powder metallurgy should be considered for possible scale-production.

In the literature, the feasibility of the mechanical properties for orthopedic implants of porous Ti-Nb-Sn alloys has been demonstrated [29–35]. The Ti-Nb-Sn system is a non-toxic alternative with low-elastic moduli for medical implants. However, the Nb and Sn content should be thoughtfully considered to stabilize the β phase without interfering in its possibility to transform to α" martensite with the application of stress. The high strength and low elastic modulus achieved in Ti-Nb-Sn alloys is related to the occurrence of stress-induced martensitic transformation and its reverse transformation [33]. The addition of Nb and Sn decreases the maximum martensitic transformation strain [32]. For the present study, 34 and 6 wt.% of Nb and Sn were chosen to promote the stabilization of β phase, respectively [36]. From the literature, the Ti-34Nb-6Sn alloy with 5% to 27% porosity, elaborated by resistance-based sintering (ERS) [36] and vacuum hot pressing and sintering [24,37,38], is a feasible material for orthopedic implants. However, the difficulties of producing near-net-shapes using those techniques should be considered for possible scale-production [39]. Previous reports showed acceptable corrosion performance of the porous Ti-34Nb-6Sn in Ringer Hartmann's and Hank's solutions for performing as a biomaterial [36,37]. Besides, an adequate biological behavior due to good compatibility and promotion of osteogenic differentiation of stem cells derived from equine bone marrow has been proven for the porous Ti-34Nb-6Sn alloy [37,38]. The hardness and compressive strength of the porous Ti-34Nb-6Sn alloy with different α and β contents are adequate for implant applications [24,38]. Furthermore, the elastic limit measured by the impulse excitation technique in the porous Ti-34Nb-6Sn alloy showed values from 41 to 63 GPa [24], which are close to those reported for the cortical bone between 10 and 30 GPa [30]. Considering those promising results for the porous Ti-34Nb-6Sn alloy, further research related to other key factors for the performance of biomaterials is necessary. Examples of those factors are the toxicity potential that can be assessed by ion release, the corrosion performance to evaluate the degradability of material in simulated biological environments, as well as a more detailed mechanical performance that considers the formability and the nature of the elastic behavior. Besides, testing different sintering conditions than those already tested is important to guide the design of future Ti-Nb-Sn biomaterials.

This work aims to evaluate the feasibility of the Ti-34Nb-6Sn alloy as a biomaterial for medical implants. Microstructural and mechanical properties, corrosion susceptibility and ion release tests were performed in two porous Ti-34Nb-6Sn alloys produced by two different compaction pressures (100 (condition A) and 200 MPa (condition B)). Using a low compact pressure could promote the formation of highly porous samples and avoid excessive grain growth. Based on this, we used a low compact pressure to verify the influence on the microstructure and consequently on the mechanical and corrosion behavior. In the literature, better biocompatibility of metallic pore implants has been demonstrated, which decreases the elastic modulus and can improve the osteointegration process, making the bone cells grow into the pores and then promote better stability with the bone. Besides, the use of a low compaction pressure could assist in the cost-benefit of the elaboration process of the alloy [39]. The mechanical, corrosion and ion release performances were explained in terms of the microstructural features of these alloys.

2. Materials and Methods

2.1. Materials' Preparation

Elemental powders of Ti (ASTM F67), Nb (99.99%) and Sn (99.50%) were purchased from Acnis do Brasil (Sorocaba-SP-Brazil), CBMM (Araxá-MG-Brazil) and Metalpó (São Paulo-Brazil) and weighed according to the predetermined stoichiometric composition of the Ti-34Nb-6Sn (wt.%) alloy. The powders were milled at room temperature in a high-energy planetary mill (FRITSCH-Pulverisette 5) in chromium steel for 40 min at 200 rpm in Ar atmosphere. The ball to powder ratio (BPR) used for the milling process was 10:1. After milling, the

powders were dried under vacuum and compacted uniaxially in a matrix (1 cm^2) with 100 (condition A) and 200 MPa (condition B). The sintering was carried out in a high vacuum-resistive furnace (COMBUSTOL-Tubular furnace) coupled to a mechanical pump (Edwards) and diffuser (Edwards). Before sintering, the furnace chamber was filled with argon and evacuated twice. The process was executed in two cycles: the first one at 450 °C for 2 h and the second one at 900 °C for 2 h under a vacuum atmosphere with a pressure of 10^{-2} Pa. The sintering was followed by furnace cooling. The metallographic preparation consisted of the following steps: The samples were embedded in resin and heated at 180 °C for 3.5 min at a pressure of 350 bar. Then, 6 min of cooling occurred. The embedded materials were sanded in a metallographic sander (Stru-ers-Labopol-25) at 150 rpm using a sequence of SiC 80-, 220-, 500- and 1000-mesh sandpapers, in a humid environment. Then, they were polished (Struers-Labopol-5) with a 9 μm solution (DiaMaxx) at 200 rpm, followed by a final solution of OPS (Struers) and hydrogen peroxide (Derra) (10:2). To eliminate possible contamination by this process, the samples were cleaned with distilled water (18.2 MΩ cm) and ethyl alcohol/acetone for 1 h in an ultrasonic bath (Elma S30 H). The preparation of the samples was carried out to promote an adequate surface for the evaluation of its microstructure, in addition to the elimination of irregularities that may influence the mechanical and electrochemical tests.

2.2. Physical Characterization

For the structural characterization of the alloys, the identification and the quantification of phases, X-ray diffraction (DRX) (Bruker/D2Phaser, Karlsruhe, Germany)) was carried out. The radiation used was Cu Kα, with λ = 0.15418 nm at 30 kV and 10 mA. The measurements were performed between 30° and 90°, with a step size of 0.02° and a scanning speed of 0.02° s^{-1}. The refinement of the structure and the quantitative analysis of the phases, as well as the treatment of the data, were carried out by the free MAUD software (version 2.94, Trento, Italy) and plotted using OriginPro software (version 8.5, Northampton, MA, USA). The porosity and phase percentages were characterized by the difference in contrast through Optical Microscopy (OM) (Nikon-ECLIPSE LV100DA-U, Melville, NY, USA) and Field Emission Scanning Electron Microscopy (FE-SEM) (ZEISS-ULTRA 55, Oberkochen, Germany) with backscattered electrons (BSE) and secondary electrons (SE), and the working conditions were E_0 = 20 kV, with a work distance of 6.3 mm. The geometric parameters such as density and porosity were investigated by the Archimedes method according to the ASTM B328 standard.

2.3. Mechanical Properties by Compressive Test

Compressive tests were carried out on cylindrical samples with a diameter and height of 10 and 7 mm at room temperature at a constant cross speed of 0.5 mm/min, employing a SHIMADZU-AG-X plus, Tokyo, Japan 100 kN universal testing machine. The materials were tested up to 2 mm of displacement. Therefore, the curves were plotted up to 0.30 mm/mm, which corresponds to approximately 2% of deformation. The proof stress at 0.2% strain was considered as the elastic limit on the stress–strain compression curves. The proof stress criterion is accurate for compression tests in several alloys, including Ti alloys [40,41]. The elastic modulus (E), yield strength (YS) and the strain-hardening coefficient (n) were calculated from the stress–strain curves. For the E, the fitted curve was calculated to the linear elastic zones. For the n, the fitted curve was calculated from the beginning of the plastic zone on the log-log true stress versus true strain. The average compressive strength for each condition was determined. The calculations and the plots were obtained using OriginPro 8.5 software. The average of five compressive strength measurements for each condition was determined.

2.4. Corrosion Susceptibility and Ion Release Evaluation

The samples, after being embedded in methacrylate, were painted on their borders with transparent enamel to delimit the attack region of the ionic solution and so that the

liquid did not enter the extremities. Then, the dimensions of all samples were measured. Three measurements were made on one side and three on the other side and the average was taken, calculating their areas. Subsequently, 50 mL of the Fusayama solution was added to sterile bottles and all samples (n = 3) were added. All of them were kept for 730 h at 37 °C. To quantify the release of the constituent ions of the alloy (Ti, Nb and Sn), the liquids were taken for analysis by Atomic Absorption Spectroscopy of Hardened Plasma coupling (ICP-OES) (Varian 715-S, Austin, TX, USA). The wavelengths used to determine the content of ions released in the solution were: 336.0 nm (Ti), 313.1 nm (Nb) and 189.9 nm (Sn).

The corrosion study was carried out by a potentiostat/galvanostat (Metrohm potentiostat-PGSTAT204, Utrecht, Netherlands), on a surface of 0.785 cm^2, using a three-electrode cell in a Fusayama solution (NaCl 0.4 g/L, KCl 0.4 g/L, $CaCl_2$ 0.8 g/L, H_2PO_4 0.7 g /L, NaF 2.5 g /L, Na_2S 0.005 g/L and Urea 1g/L) at 37 °C. The Ag/AgCl and platinum electrodes were used as reference and auxiliary electrodes, respectively. The electrochemical tests consisted of the open-circuit potential (OCP) measurement (for 30 min) and the polarization curves under 2 mV/s. The corrosion parameters were determined by Tafel's extrapolation methods using Wolfram Mathematica 12.1 software. The curves were also made in OriginPro 8.5 software and three samples per condition were studied.

The corrosion rate (Cr) was calculated to take into account the value of i_{corr} of each condition, as well as the alloy density and the valence electrons of Ti (n).

The equation used for this was:

$$Cr = \frac{M\, w\, i_{corr}}{F\, n} \quad (1)$$

Then, the value was multiplied by 1,314,000 s (1 year), which affords the corrosion resistance in μm/year.

3. Results and Discussion

In Figure 1a, the x-ray diffraction (XRD) profiles of powders Ti, Nb and Sn compared to samples in conditions A and B are shown. The constituent phases of the A and B conditions are present in the XRD profiles of Figure 1a. The peaks showed the presence of α and β phases and no peaks reminiscent of Ti, Nb or Sn were found. Considering that the crystalline structure of β and Nb phases corresponds to the space group Im-3m and their lattice parameters are nearly similar [20,21], it is not possible to discern between both phases by XRD. The three phases present are in agreement with those expected for Ti-Nb alloys with a similar Nb content obtained by powder metallurgy methods [22–24]. It is worthy to note that the intensity of peaks (002) and (101), i.e., second and third peaks, of α phase in condition B decreased slightly when compared to condition A. Simultaneously, there is an increment in the intensity of the peak (200) of β phase (second peak around 55.7°), suggesting the unceasing transformation of phases with the increment of compaction pressure. These results are in accordance with those obtained by Rietveld refinement, which showed a higher formation of β phase with the increment of compaction pressure, i.e., 73.1% ± 1.2% and 79.9% ± 0.1% for conditions A and B, respectively. The increment of β phase in condition B might be related to the higher solubilization of Nb (β stabilizer) resulted from the higher compaction pressure. Other authors [25] have reported similar behavior of the β phase by varying the compaction pressure of the Ti-Al-8V-5Fe alloy.

Figure 1b,c show the morphology and size of phases and pores in conditions A and B. Through the difference in contrast by using backscattered electron (BSE) signals, the differences in the chemical composition of the phases become visible. Regions with a dark contrast indicate the presence of the element with the highest atomic mass on the alloy, i.e., Sn, which is mainly solved in the α phase. The gray contrast denotes regions rich in Nb and Ti, that is, β + α phases, while particles of pure Nb generate a white contrast. The microstructure of both conditions was formed by α, β, as well as Nb particles that did not diffuse through the material. In agreement with the above-mentioned phase percentages,

the α phase in both microstructures is visibly less frequent than the β phase. The white contrast regions are present in 53.4% and 57.1% in conditions A and B, respectively, with an increment of 7% according to the image analysis. It is also noticeable that the average size of Nb particles is 9.5 ± 1.8 µm. These particles consist of a pure Nb core surrounded by a biphasic (α + β) microstructure. The existence of such Nb particles could be related to an insufficient sintering temperature, which was not enough to obtain a total diffusion of Nb into the matrix. It has been reported that a total diffusion of Nb into the β matrix is obtained by using sintering temperatures above 1600 °C [26]; nonetheless, the employment of such temperature in the current system could affect the content of Sn in the alloy. Besides, the increment of β phase in condition B might be related to the higher solubilization of Nb (β stabilizer) resulted from the higher compaction pressure.

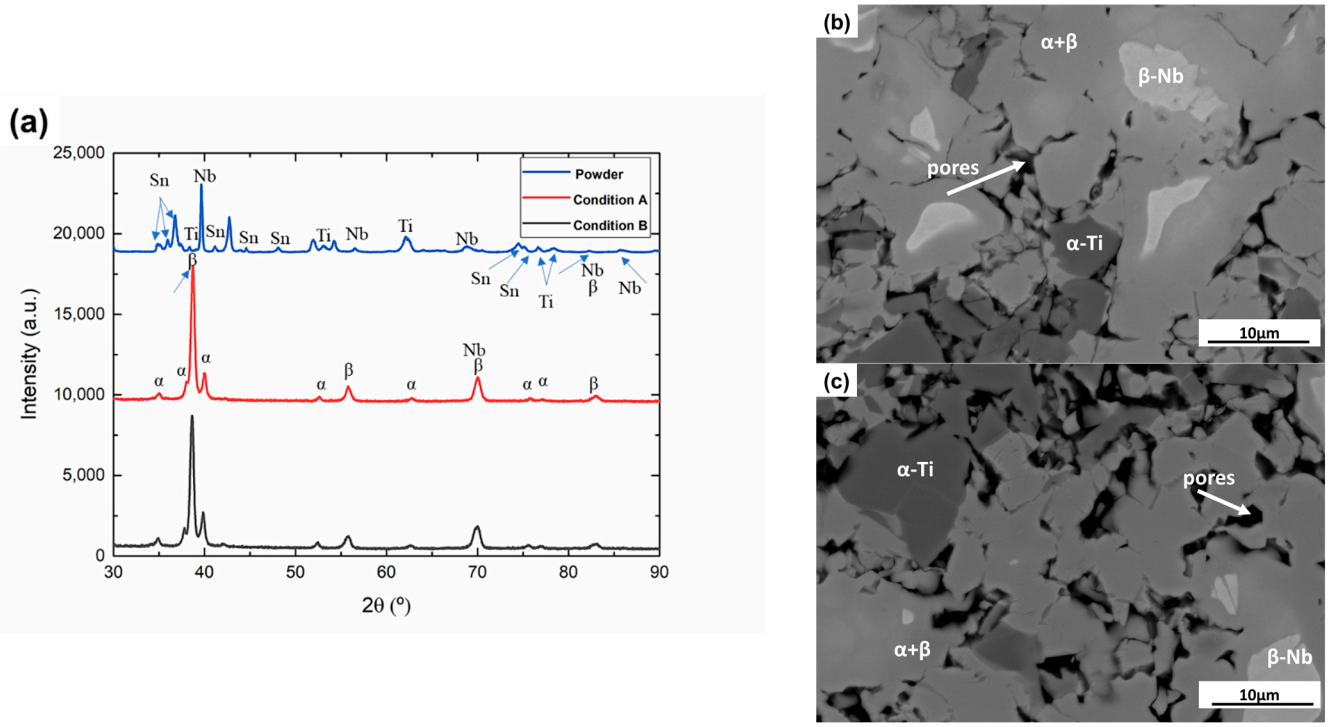

Figure 1. (**a**) XRD patterns for milled powder and samples sintered in conditions A and B, as well as SEM micrographs by BSE detector of (**b**) condition A and (**c**) condition B.

From SEM images, there was no evident change in porosity distribution, morphology or size. The previous statement was corroborated by the data included in Table 1, which showed a slight decrement in porosity (from 25% to 22%) when increasing the compaction pressure. This result was also congruent with the nearly similar experimental densities from 4.02 to 4.24 g/cm^3 for conditions A and B, respectively. Such decrement in porosity could be triggered by the higher contact frequency between the powder particles when increasing the compressibility forces. Furthermore, according to different authors, the vacancies formed (due to the release of hydrogen) during the sintering process might contribute to the densification process [42,43].

Table 1. Density and total porosity measured by the Archimedes method for the studied materials' conditions.

Condition	Compaction Pressure (MPa)	Experimental Density (g/cm^3)	Relative Density, ρ/ρ_s	Total Porosity (%)
A	100	4.02 ± 0.11	0.73 ± 0.01	26 ± 0.8
B	200	4.24 ± 0.07	0.78 ± 0.02	22 ± 0.5

Figure 2 shows the compressive true stress–true strain curves of sintered conditions A and B. Both conditions exhibited similar compressive behaviors. According to the mechanical properties shown in Table 2, yeld strength (*YS*) values were in the range from 245 to 318 MPa for conditions A and B, respectively. These YS values are higher than those of bones, which have been reported between 104 and 121 MPa [44]. Compared to the *YS* value (~1190 MPa) of Ti-60Mo with a porosity of about 27% [45], the *YS* values obtained in both conditions A and B are low. This can be related to the phase content; while the reported Ti-60Mo has a homogeneous β phase microstructure, conditions A and B have at least 20% of α phase. It is well-known that the β phase has a higher mechanical performance than the α phase [26]. The strong effect of the α phase in the *YS* of Ti alloys can be confirmed by the obtainment of ~100 to 110 MPa in an α phase Ti-O-Fe-Ni-C-H alloy with ~30% porosity [46]. The ultimate strength before fracture was ~590 and 660 MPa for A and B conditions, respectively. Such increments of mechanical resistance with the compaction pressure might be related to the greater density of condition B in comparison with that for the A material. The *E* values of both materials (from 14 to 19 GPa) are within those reported for cortical bone, between 10 and 30 GPa [45,47], which might be an important advantage for its use as an implant biomaterial. It has been reported that reducing the mismatch of *E* between the implant and the bone reduces the overload of the bone (stress-shielding) and increases the success rate for osseointegration [48]. This suggests a satisfactory mechanical performance of Ti-34Nb-6Sn in the human body. Besides, the *E* values obtained for the Ti-34Nb-6Sn alloy are well below those reported for numerous biomedical alloys, such as commercially pure Ti, Ti-35Nb-72Zr-5Ta, Ti-15Mo-5Zr-3Al, Ti-6Al-7Nb and Ti-6Al-4V, among others [49]. There is also a remarkably clear tendency towards increasing *E* with the compaction pressure, suggesting that the obtainment of low *E* values could be related to the low compaction pressures employed in this work. The previous statement was corroborated by the highest *E* values (~105 to 112 GPa) of Ti-16Nb-2Sn and Ti-16Nb-4Sn by powder metallurgy methods with a compaction pressure of 400 MPa [33,50]. The porous Ti-34Nb-6Sn also has the lowest *E* value in comparison with the other Ti-10 to 43 wt.% Nb-2 to 15 wt.% Sn alloys prepared by arc melting [17,30,51–53]. These results also corroborate the strong influence of the porous microstructure on the suitability of mechanical properties for biomaterials. Porosity has already been reported as a promising parameter to reduce the *E* values of metallic biomaterials [52]. It should also be noted that there was a greater influence of density on the *E* value, in comparison with the effect of the phase percentages. Considering that the β-Ti phase is known for its low *E* values [30,54], the increment of β phase in condition B was expected to decrease the value of *E*. Nevertheless, the *E* increased with the compaction pressure, which could be the result of higher density and bond strength. Other authors have also reported low *E* values (~25 to 0.5 GPa) in α-Ti with porosity greater than 50% [55].

Figure 2a also allows for observing the formation of cracks that appeared from the onset of the plastic deformation region, being a result of the typical barreling during compression tests [56]. The formation of cracks in the corners of compression test samples and their propagation towards the center is widely reported for different metallic materials, including Ti alloys [57]. This phenomenon is related to the heterogeneous distribution of pressure as a function of the radial distance from the center to the corners in compression test samples [56]. The center of the tested sample concentrates the higher stress, generating the formation of cracking at the corners, with the corners being the zones with a lower compromise of mechanical integrity for the whole sample [58]. In the present study, the cracking in both conditions A and B behaved similarly. The formation of radial cracking started at about 2.3 mm from the center of each tested condition. Due to their similar fracture modes, the insert in Figure 2a is representative of the behavior of both studied conditions, A and B.

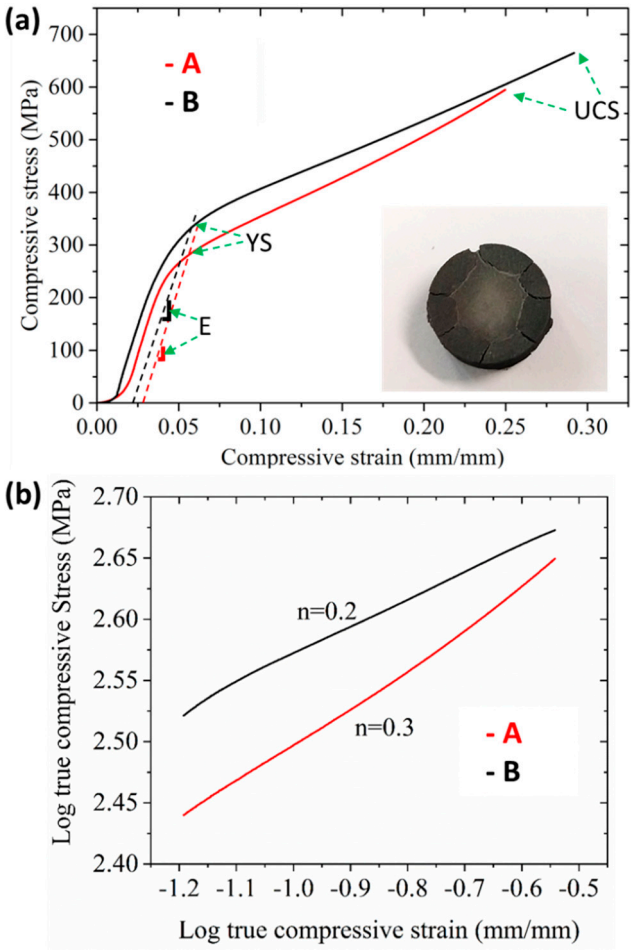

Figure 2. (**a**) Stress versus strain plots from the compression tests applied to conditions A and B, including a representative photograph of the fracture, and (**b**) log true stress versus log true strain of the plastic zone to determine the strain-hardening coefficient (*n*).

Table 2. Mechanical properties obtained from the compression test.

Condition	Elastic Modulus, *E* (GPa)	Yield Strength, *YS* (MPa)	Strain-Hardening Coefficient, *n*	Ultimate Compressive Strength, *UCS* (MPa)	Specific Elastic Modulus, E/ρ_s
A	14.1 ± 3.7	244.9 ± 33.7	2.7 ± 0.2	590.0 ± 75.7	3.6 ± 0.5
B	18.8 ± 7.2	318.6 ± 45.5	4.8 ± 0.9	660.0 ± 93.1	4.4 ± 0.6

Furthermore, Figure 2b shows the estimation of the strain-hardening coefficient (*n*) from the slope of the logarithmic true stress versus logarithmic true strain. It is well-known that *n* is a measure of the capability of the material to gain strength while it is being deformed. It can be seen that the higher value of *n* in condition A (*n* = 0.3) suggests great formability in comparison with condition B. This result could be expected from the increment of strength in condition B. Such increment of mechanical resistance could result from the augmentation of dislocation density on material B, which simultaneously decreases the free path for deformation, triggering the decrement of ductility.

The representative morphology of failure from the compression test was observed by FE-SEM and is displayed in Figure 3a. The failure follows the path of the grain boundaries, i.e., the typical failure for the studied alloys is intergranular. It is well-known that the presence of second phases on the grain boundaries, as well as the presence of pores, promotes intergranular cracking [59]. Based on the above, the presence of Nb particles and the porous microstructure of both conditions were responsible for this fracture morphology.

In the magnification of Figure 3b, it is possible to observe the preferential path of the crack along with the position of Nb particles.

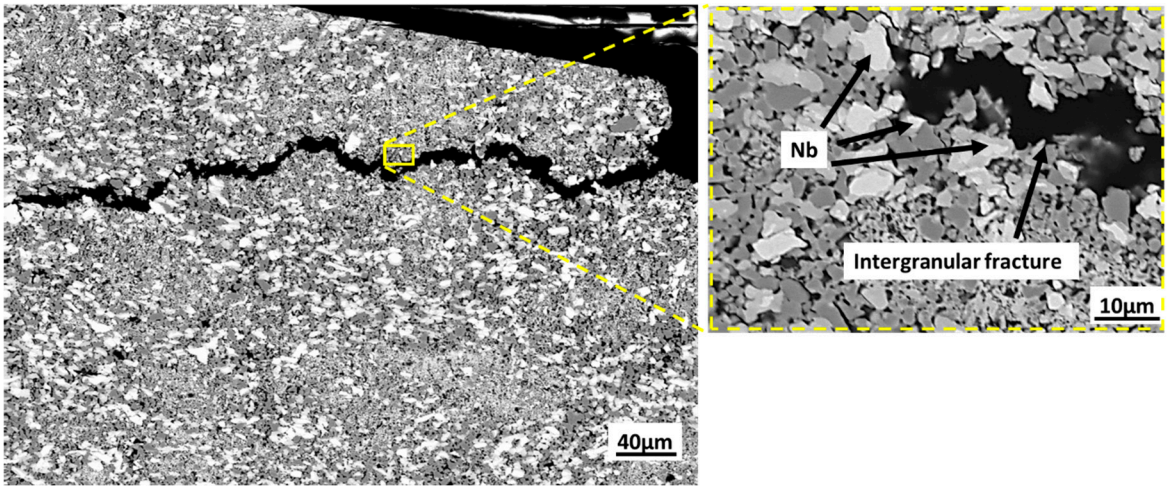

Figure 3. FE-SEM micrograph at (**a**) lower and (**b**) higher magnification of the fracture generated by the compression test. The morphology of the presented fracture is representative of both conditions A and B.

The release of Ti, Nb and Sn ions from conditions A and B is shown in Figure 4. The quantity and rate of ion release for both studied conditions are detailed in Table 3. Condition B released a greater quantity of the three elements present. However, the Nb ions' release between 1.4 and 2.9 µg cm^{-2} day^{-1} is well below the Nb content in a diet of 100 g of protein, 250 g of carbohydrate and 100 g of fat, which is about 620 µg [60]. Regarding the Sn, it has been suggested at a maximum content of 200 mg/kg of food [61]. Such values are above the Sn ions' release obtained for both conditions (0.89 to 1.45 µg cm^{-2} day^{-1}). Additionally, the Food and Drug Administration (FDA) recommends an upper limit of 1% of Ti from the total mass of ingested food [62]. This is a maximum of 106 µg of TiO_2 per kg of food. Considering the total mass of 1 L of Fusayama solution used for the ion release tests, the Ti ions' release from both conditions was 0.018% (condition A) and 0.021% (condition B). Previous results allowed considering that all the ion release concentrations are within the acceptable ranges for human ingestion.

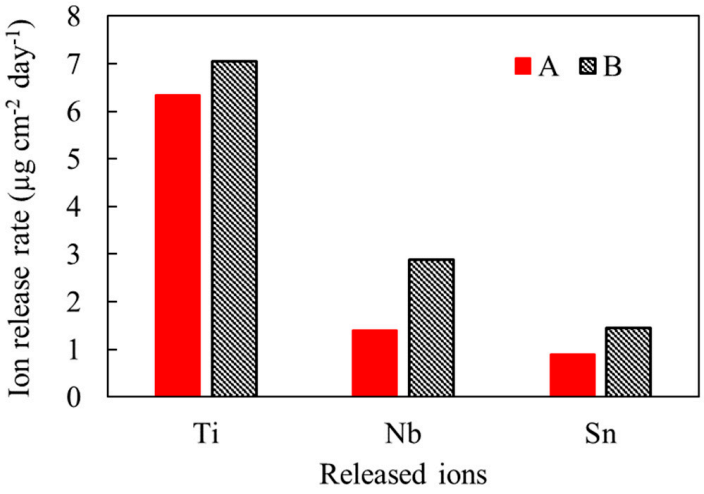

Figure 4. Ti, Nb and Sn ions' release from conditions A and B.

Table 3. Ti, Nb and Sn ions released compared with the nominal composition of the alloy.

Condition	Units	Ti	Nb	Sn	Total
A	µg/L	556 ± 386	123 ± 13.7	72 ± 27	751
	µg cm^{-2} day^{-1}	6.35 ± 0.12	1.40 ± 0.12	0.89 ± 0.33	8.64
	%	74	16	10	100
B	µg/L	618 ± 144	253 ± 150	117 ± 89	988
	µg cm^{-2} day^{-1}	7.05 ± 0.39	2.88 ± 0.52	1.45 ± 0.43	11.44
	%	62	26	12	100

Moreover, the percentages of Ti and Sn release (62% to 74% and 10% to 12%) were higher than their percentages in the nominal composition of the alloy (60% and 6%). Contrarily, Nb ions' release values from both conditions (16% to 26%) were lower than the nominal percentage (34%). From these results, the alloy suffered a preferential chemical attack in the solid solution in comparison with the Nb immiscible particles. Previous phenomena could be related to the well-known lattice distortion and binding energy changes resulted from the introduction of substitutional or interstitial elements into the atomic arrangement of the solid solution [63]. It was also noted that there was a higher dissolution rate of the three constituent elements on the alloy with greater compaction pressure (condition B). Interestingly, condition B also has a lower porosity percentage and higher content of beta phase in comparison with condition A. From the literature, it was found that the presence of pores increases the trapping of electrolyte species and the decrement of oxygen supply, which is essential for the stability of the passive film [64]. Based on the above, the increment of the ion release rate with the decrement of total porosity on the Ti-34Nb-6Sn alloy was a non-expected result. It also should be pointed out that the greater presence of the β phase in condition B implies a greater percentage of solubilized Nb. Considering that the Nb particles showed less chemical susceptibility than the solid solution, the great ion release rate from condition B could be triggered by the decrement of Nb cores. Previous results suggest that the ion release in the porous Ti-34Nb-6Sn alloy was mainly influenced by the solid solution percentage in comparison with the lower effect of porosity. The β-type grains suffered the greatest attack by immersion, due to lower density and higher atomic disorder [65,66]. The highest ionization energy of Sn in comparison with that of Ti and Nb also supports the preferential attack of the β phase (rich in Nb) [67]. The Nb cores dispersed along the microstructure of both conditions showed greater resistance to the corrosive media of artificial saliva.

Electrochemical analyses were performed by evaluating the open-circuit potential (OCP) and the potentiodynamic polarization curves (PPC), and the results are displayed in Figure 5. The kinetic parameters obtained from the corrosion test are shown in Table 4. Figure 5a shows the open-circuit potential (OCP) curves of both studied conditions. Both conditions showed similar tendencies, i.e., the corrosion potential augmented progressively at the early stage of immersion, and then remained almost constant at immersion times above 1100 s. In both conditions, the initial OCP showed negative values, which indicates that the ground base alloy was active. The continuous increase of potential during the tests indicated the formation of a passive oxide film at the surface of both conditions of the alloy [68]. Nevertheless, condition A showed a more negative corrosion potential in comparison with condition B. Compared to the OCP values from –0.04 to –0.07 V after 2100 s of immersion of Ti-34Nb-6Sn obtained by ERS in Ringer Hartmann's solution, the OCP of conditions A and B indicated higher corrosive activity at the surface. This can be related to the severity of the corrosive medium used for testing. While the Ringer Hartmann's solution has a pH between 6 and 7 [36], the Fusayama solution with the chemical composition as used in this study has a pH of 5.270 ± 0.108 [37,69].

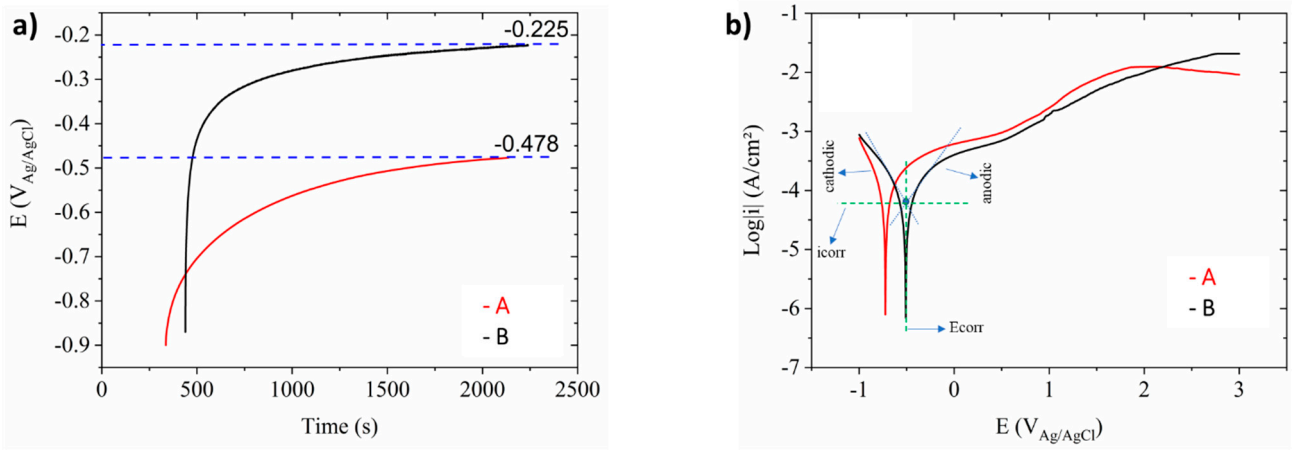

(**a**) (**b**)

Figure 5. Electrochemical corrosion behavior of both studied conditions: (**a**) open-circuit potential (*OCP*) and (**b**) potentiodynamic polarization curves (*PPC*).

Table 4. Kinetic parameters obtained from the PPC.

Condition	Corrosion Current Density, I_{corr} (A/cm^2)	Corrosion Potential, E_{corr} (V)	Polarization Resistance, Rp (kΩ)	Corrosion Rate (μm/year)
A	1.62×10^{-5}	−0.72	1.55	1.14
B	1.05×10^{-5}	−0.5	2.39	0.74

The differences in phase content could also play a key role in the different electrochemical behavior between both studies. The Ti-34Nb-6Sn obtained by ERS has more than 96% of β phase [36], while the β phase in the present study ranges from 73% to 79%. It is known that β-Ti alloys have better resistance in corrosive environments such as oral or body fluids. However, this is mainly related to the content of β stabilizers such as Mo or Zr, which decrease the corrosion potential of Ti alloys [70,71]. As Mo and Zr were not included in the ERS Ti-34Nb-6Sn alloy from the literature, its better corrosion performance might be related to the decrement of α/β interfaces' density compared to that of the conditions A and B of this study. The α/β interfaces are preferential sites for corrosion attack due to the different rates of passive film formation between both phases [71,72]. On the other hand, compared to the *OCP* value (-0.7 V) of Ti-34Nb-6Sn sintered at lower temperature and time conditions than those used in this study [37], the *OCP* values of both conditions A and B are less prone to corrosion. This can also be related to the phase content and resultant α/β interfaces' density. The Ti-34Nb-6Sn from the literature reported 55% of β phase [37], from which a higher density of α/β is expected compared to the A and B conditions from this study. Furthermore, the *OCP* values and passive formation tendency of both conditions A and B are similar to those reported for different Ti-Nb alloys, such as Ti-30Nb, Ti-30Nb with 2 to 10 wt.% Sn and Ti16-Nb30-SH [29,73].

Figure 5b compares the potentiodynamic polarization curves of conditions A and B. Both curves show typical regions of a metallic material, referring to the cathodic region of the polarization curve, which are: active and tending to the passivation zone. Condition A has a passive potential in the range of −0.720 to −0.563 V (Ag/AgCl) and material B in the range of −0.508 to −0.276 V (Ag/AgCl). Both materials have low current density values that do not exceed log |5| (A/cm^2). The PPC of both conditions suggested the formation of a superficial passivation film. This was observed through the decrement of current density and the significant posterior increment. This behavior displayed a greater intensity in condition A. As seen in Table 4, the average corrosion potential for condition A is lower than that for condition B, with an increment of around 36% in material B. These average potentials obtained by the polarization curves were significantly lower than those obtained by the *OCP* measurements. This phenomenon can be explained by

the nature of the executed polarization test. The starting cathodic potentials applied to samples could partially remove the passive oxide film. Comparing with condition A, the polarization resistance (*Rp*) increased 1.5 times in condition B. Thus, the condition produced by the higher compaction pressure showed higher corrosion resistance. The differences in porosity between both conditions generated a noticeable difference in the corrosion potential values. It has been reported that the increment of porosity increases the corrosion susceptibility on Ti-Nb and Ti-Nb-Sn alloys [64,74]. Based on the above, it was expected to find a better corrosion performance from the condition with a lower total porosity percentage (condition B).

The highest content of β phase in condition B (79.9% ± 0.1%) compared to that in condition A (73.1% ± 1.2%) could also contribute to its improvement of corrosion resistance by decreasing the density of α/β interfaces. Compared to the literature, the E_{corr} of conditions A and B (−0.5 to −0.72 V) is lower than that reported for the Ti-34Nb-6Sn sintered at a lower temperature and time (−0.78 V) [37]. As explained before, this improvement in electrochemical behavior might be related to a lower α/β interface density in the conditions A and B compared to that obtained by 55% of β phase in the literature [37]. The different corrosive testing media might also influence the corrosion behavior: the Ti-34Nb-6Sn from the literature was tested in Hank's solution (pH from 4 to 7) [37], while the media used in this study was artificial saliva (pH = 5.27). Moreover, the E_{corr} (−0.4 to −0.47 V) of the Ti-34Nb-6Sn elaborated by electrical resistance sintering (ERS) [36] suggested a higher corrosion resistance compared to both conditions in this study. However, as was explained before, the lower severity of the Ringer Hartmann's solution of that study compared to the artificial saliva used in this work might strongly influence the result.

Considering a typical corrosion rate for metallic materials in the range of 25 to 100 μm/year [75], both studied materials exhibited excellent corrosion rates (0.74 to 1.14 μm/year). Moreover, condition B presented greater corrosion resistance than condition A. It is remarkable that, in both studied conditions, the rupture of the passive film occurred close to 980 mV/Ag/AgCl. The human body has a reduction/oxidation potential of 500 mV/Electrostatic chuck (SCE) [76]. Therefore, the potential of both conditions meets the requirements for good electrochemical performance in the human body.

4. Conclusions

The porous Ti-34Nb-6Sn alloy was produced by using two different low compaction pressure conditions (100 MPa (condition A) and 200 MPa (condition B). The microstructural, mechanical, electrochemical and ion release behaviors allowed for obtaining the following conclusions:

1. Both conditions, A and B, were mainly constituted by α, β and Nb phases. Condition B showed a slight increment of β phase content and decrement of total porosity.
2. In comparison with condition A, the mechanical assessment showed increments of 30% and 12% of the yield and ultimate strength in condition B, respectively. The *YS* values for both conditions (245 to 318 MPa) were above those reported for human bone. The elastic moduli of both conditions (14.06 to 18.82 GPa) were similar to those reported for cortical bone.
3. After the immersion in Fusayama artificial saliva, both conditions showed levels of Ti, Nb and Sn ions' release within the acceptable ranges for the human body. The presence of Nb particles distributed along the microstructure of conditions A and B could influence the occurrence of intergranular cracking during the ion release tests.
4. Through the electrochemical study of both conditions, condition B showed a lower corrosion rate (0.74 μm/year) in comparison with condition A (1.14 μm/year). This could be related to the lower total porosity percentage in condition B.
5. Based on the previous results, both conditions showed adequate mechanical, ion release and corrosion performance for being employed as biomaterials for orthopedic implants. Specific tests must be performed in different environments to determine the performance of this alloy in different areas of the human body.

Author Contributions: Conceptualization, M.C.-R. and V.A.-B.; methodology, M.C.-R.; validation, V.A.-B.; formal analysis, M.C.-R.; investigation, M.C.-R.; data curation, M.C.-R. and L.R.-R.; writing—original draft preparation, M.C.-R.; writing—review and editing, L.R.-R., D.L.-B., F.S.-L. and V.A.-B.; supervision, A.L.G.-A. and V.A.-B.; project administration, M.C.-R., A.L.G.-A. and V.A.-B.; funding acquisition, A.L.G.-A. All authors have read and agreed to the published version of the manuscript.

Funding: This research was funded by the Fundação de Amparo à Pesquisa do Estado de São Paulo (FAPESP) (grant: 2017/13876-2; 2019/24237-6), by the Ministerio Español de Ciencia, Innovación y Universidades, with Grant RTI2018-097810-B-I00, and by the Instituto de Pesquisas Tecnológicas do Estado de São Paulo (IPT-SP). L.R.-R. acknowledges CONACyT for the PhD scholarship with number 465504.

Informed Consent Statement: Not applicable.

Data Availability Statement: The raw data related to this manuscript can be made available upon request.

Conflicts of Interest: The authors declare no conflict of interest.

References

1. Lewallen, E.A.; Riester, S.M.; Bonin, C.A.; Kremers, H.M.; Dudakovic, A.; Kakar, S.; Cohen, R.C.; Westendorf, J.J.; Lewallen, D.G.; van Wijnen, A.J. Biological Strategies for Improved Osseointegration and Osteoinduction of Porous Metal Orthopedic Implants. *Tissue Eng. Part B Rev.* **2015**, *21*, 218–230. [CrossRef]
2. Geetha, M.; Singh, A.K.; Asokamani, R.; Gogia, A.K. Ti based biomaterials, the ultimate choice for orthopaedic implants–A review. *Prog. Mater. Sci.* **2009**, *54*, 397–425. [CrossRef]
3. Kulkarni, M.; Mazare, A.; Schmuki, P.; Iglic, A. Biomaterial surface modification of titanium and titanium alloys for medical applications. *Nanomedicine* **2014**, *111*, 111–136.
4. Davis, J.R. *Handbook of Materials for Medical Devices*, 4th ed.; ASM International: Novelty, OH, USA, 2006.
5. Niinomi, M.; Narushima, T.; Nakai, M. *Advances in Metallic Biomaterials*, 3rd ed.; Springer: Berlin/Heidelberg, Germany, 2015.
6. Churakova, A.; Gunderov, D.; Lukyanov, A.; Nollmann, N. Transformation of the TiNi Alloy Microstructure and the Mechanical Properties Caused by Repeated B2-B19′ Martensitic Transformations. *Acta Met. Sin. Engl. Lett.* **2015**, *28*, 1230–1237. [CrossRef]
7. Liu, X.; Chu, P.K.; Ding, C. Surface modification of titanium, titanium alloys, and related materials for biomedical applications. *Mater. Sci. Eng.* **2004**, *47*, 49–121. [CrossRef]
8. De Vasconcellos, L.M.R.; Rodarte, Y.; Prado, R.F.D.; de Vasconcellos, L.G.O.; Graa, M.L.D.A.; Cairo, C.A.A. Porous Titanium by Powder Metallurgy for Biomedical Application: Characterization, Cell Citotoxity and in vivo Tests of Osseointegration. *Biomed. Eng.-Techn. Appl. Med.* **2012**. [CrossRef]
9. Cremasco, A.; Messias, A.; Esposito, A.R.; Duek, E.A.D.R.; Caram, R. Effects of alloying elements on the cytotoxic response of titanium alloys. *Mater. Sci. Eng. C* **2011**, *31*, 833–839. [CrossRef]
10. Barceloux, D.G. Vanadium. *J. Toxicol. Clin. Toxicol.* **1999**, *37*, 265–278. [CrossRef]
11. Marquis, J.K. Aluminum neurotoxicity: An experimental perspective. *Bull. Environ. Contam. Toxicol.* **1982**, *29*, 43–49. [CrossRef]
12. Merritt, K.; Brown, S.A. Effect of proteins and pH on fretting corrosion and metal ion release. *J. Biomed. Mater. Res.* **1988**, *22*, 111–120. [CrossRef]
13. Williams, R.; Brown, S.A.; Merritt, K. Electrochemical studies on the influence of proteins on the corrosion of implant alloys. *Biomaterials* **1988**, *9*, 181–186. [CrossRef]
14. Black, J. Part III Host Response: Biological Effects of Implants. In *Biological Performance of Materials*; CRC Press: Boca Raton, FL, USA, 2005; pp. 157–354.
15. Hench, L.; Ethridge, E. Biomaterials—The Interfacial Problem. In *Advances in Biomedical Engineering*; Academic Press: Cambridge, MA, USA, 1975; pp. 35–150.
16. Biesiekierski, A.; Wang, J.; Abdel-Hady Gepreel, M.; Wen, C. A new look at biomedical Ti-based shape memory alloys. *Acta Biomater.* **2012**, *8*, 1661–1669. [CrossRef] [PubMed]
17. Miura, K.; Yamada, N.; Hanada, S.; Jung, T.-K.; Itoi, E. The bone tissue compatibility of a new Ti–Nb–Sn alloy with a low Young's modulus. *Acta Biomater.* **2011**, *7*, 2320–2326. [CrossRef] [PubMed]
18. Matsumoto, H.; Watanabe, S.; Hanada, S. Beta TiNbSn Alloys with Low Young's Modulus and High Strength. *Mater. Trans.* **2005**, *46*, 1070–1078. [CrossRef]
19. Chen, X.-B.; Li, Y.; Hodgson, P.D.; Wen, C. The importance of particle size in porous titanium and nonporous counterparts for surface energy and its impact on apatite formation. *Acta Biomater.* **2009**, *5*, 2290–2302. [CrossRef] [PubMed]
20. Okamoto, H.; Massalski, T.B. Binary alloy phase diagrams requiring further studies. *J. Phase Equilibria Diffus.* **1994**, *15*, 500–521. [CrossRef]
21. Salvo, C.; Aguilar, C.; Cardoso-Gil, R.; Medina, A.; Bejar, L.; Mangalaraja, R. Study on the microstructural evolution of Ti-Nb based alloy obtained by high-energy ball milling. *J. Alloys Compd.* **2017**, *720*, 254–263. [CrossRef]
22. Zhou, Z.C.; Du, J.; Yang, H.; Gu, S.; Yan, Y. Microstructures and Properties of Ti-Nb Alloys Produced by Powder Metallurgy. *Appl. Mech. Mater.* **2011**, *80–81*, 431–435. [CrossRef]

23. Yahaya, M.; Sahidin@salehudin, S.; Sulaiman, M.; Shah, N.H.N.E.A.; Ismail, M.H. Microstructures and Mechanical Properties of Ti-Nb Alloy at Different Composition of Nb Produced via Powder Metallurgy Route. *Mater. Sci. Forum* **2016**, *863*, 14–18. [CrossRef]
24. Rossi, M.C.; Bayerlein, D.L.; de Gouvêa, E.S.; Rodríguez, M.V.H.; Escuder, A.V.; Borrás, V.A. Evaluation of the influence of low Mg content on the mechanical and microstructural properties of β titanium alloy. *J. Mater. Res. Technol.* **2021**, *10*, 916–925. [CrossRef]
25. Zhang, Y.; Guo, X.; Chen, Y.; Li, Q. Effect of compaction pressure on the densification, microstructure, and mechanical properties of Ti-1Al-8V-5Fe alloy based on TiH 2 and HDH-Ti powders. *Micro Nano Lett.* **2019**, *14*, 906–910. [CrossRef]
26. Santos, D.R.D.; Henriques, V.A.R.; Cairo, C.A.A.; Pereira, M.D.S. Production of a low young modulus titanium alloy by powder metallurgy. *Mater. Res.* **2005**, *8*, 439–442. [CrossRef]
27. Ryan, G.; Pandit, A.; Apatsidis, D.P. Fabrication methods of porous metals for use in orthopaedic applications. *Biomaterials* **2006**, *27*, 2651–2670. [CrossRef] [PubMed]
28. Froes, F.H.; Mashl, S.J.; Hebeisen, J.C.; Moxson, V.S.; Duz, V.A. The technologies of titanium powder metallurgy. *JOM* **2004**, *56*, 46–48. [CrossRef]
29. German, R.M. *Powder Metallurgy Science*, 2nd ed.; MPIF: Princeton, NJ, USA, 1994; p. 192.
30. Moraes, P.E.; Contieri, R.J.; Lopes, É.S.; Robin, A.; Caram, R. Effects of Sn addition on the microstructure, mechanical properties and corrosion behavior of Ti–Nb–Sn alloys. *Mater. Charact.* **2014**, *96*, 273–281. [CrossRef]
31. Adiningsih, D.R.; Utomo, E.P. Anawati The microstructure and mechanical hardness of cast Ti-30Nb-5Sn after solution treatment. *IOP Conf. Ser. Mater. Sci. Eng.* **2019**, *541*, 012049. [CrossRef]
32. Sharma, B.; Vajpai, S.K.; Ameyama, K. Synthesis of Ternary Ti-25Nb-11Sn Alloy by Powder Metallurgy Route Using Titanium Hydride Powder. *Mater. Trans.* **2016**, *57*, 1440–1446. [CrossRef]
33. Cai, S.; Wang, L.; Schaffer, J.; Gao, J.; Ren, Y. Influence of Sn on martensitic beta Ti alloys. *Mater. Sci. Eng. A* **2019**, *743*, 764–772. [CrossRef]
34. Matsumoto, H.; Watanabe, S.; Hanada, S. Microstructures and mechanical properties of metastable β TiNbSn alloys cold rolled and heat treated. *J. Alloys Compd.* **2007**, *439*, 146–155. [CrossRef]
35. Li, P.; Ma, X.; Wang, D.; Zhang, H. Microstructural and Mechanical Properties of β-Type Ti–Nb–Sn Biomedical Alloys with Low Elastic Modulus. *Metals* **2019**, *9*, 712. [CrossRef]
36. Mahran, G.M.A.; Omran, A.-N.M. Fabrication of a β Ti–30Nb–4Sn Biomedical Alloy Using Mechanical Alloying. *Sci. Adv. Mater.* **2018**, *10*, 1509–1518. [CrossRef]
37. Rossi, M.C.; de Gouvêa, E.S.; Rodríguez, M.V.H.; Saeki, M.J.; Escuder, A.V.; Borrás, V.A. Study of the current density of the electrical resistance sintering technique on microstructural and mechanical properties in a β Ti-Nb-Sn ternary alloy. *Appl. Phys. A* **2021**, *127*, 796. [CrossRef]
38. Rossi, M.C.; Bayerlein, D.L.; Brandão, J.D.S.; Pfeifer, J.P.H.; Rosa, G.D.S.; Silva, W.D.M.; Martinez, L.G.; Saeki, M.J.; Alves, A.L.G. Physical and biological characterizations of TiNbSn/(Mg) system produced by powder metallurgy for use as prostheses material. *J. Mech. Behav. Biomed. Mater.* **2021**, *115*, 104260. [CrossRef]
39. Dias, C.D.S.; Rossi, M.C.; Apolonio, E.V.P.; Rosa, G.D.S.; Pfeifer, J.P.H.; Hussni, C.A.; Watanabe, M.J.; Alves, A.L.G. Low Mg content on Ti-Nb-Sn alloy when in contact with eBMMSCs promotes improvement of its biological functions. *J. Mater. Sci. Mater. Med.* **2021**, *32*, 144. [CrossRef]
40. Fang, Z.Z.; Paramore, J.D.; Sun, P.; Chandran, K.S.R.; Zhang, Y.; Xia, Y.; Cao, F.; Koopman, M.; Free, M. Powder metallurgy of titanium–past, present, and future. *Int. Mater. Rev.* **2018**, *63*, 407–459. [CrossRef]
41. Ashby, M.F.; Shercliff, H.; Cebon, D. *Engineering, Science, Processing and Design*; Katey Birtcher: Cambridge, MA, USA, 2007.
42. Imwinkelried, T. Mechanical properties of open-pore titanium foam. *J. Biomed. Mater. Res. Part A* **2007**, *81*, 964–970. [CrossRef] [PubMed]
43. Robertson, I.M.; Schaffer, G.B. Comparison of sintering of titanium and titanium hydride powders. *Powder Met.* **2010**, *53*, 12–19. [CrossRef]
44. Zheng, Y.; Yao, X.; Liang, J.; Zhang, D. Microstructures and Tensile Mechanical Properties of Titanium Rods Made by Powder Compact Extrusion of a Titanium Hydride Powder. *Met. Mater. Trans. A* **2016**, *47*, 1842–1853. [CrossRef]
45. Oh, I.-H.; Nomura, N.; Masahashi, N.; Hanada, S. Mechanical properties of porous titanium compacts prepared by powder sintering. *Scr. Mater.* **2003**, *49*, 1197–1202. [CrossRef]
46. Delvat, E.; Gordin, D.; Gloriant, T.; Duval, J.; Nagel, M. Microstructure, mechanical properties and cytocompatibility of stable beta Ti–Mo–Ta sintered alloys. *J. Mech. Behav. Biomed. Mater.* **2008**, *1*, 345–351. [CrossRef]
47. Li, F.; Li, J.; Xu, G.; Liu, G.; Kou, H.; Zhou, L. Fabrication, pore structure and compressive behavior of anisotropic porous titanium for human trabecular bone implant applications. *J. Mech. Behav. Biomed. Mater.* **2015**, *46*, 104–114. [CrossRef]
48. Niinomi, M. Mechanical biocompatibilities of titanium alloys for biomedical applications. *J. Mech. Behav. Biomed. Mater.* **2008**, *1*, 30–42. [CrossRef]
49. Brizuela, A.; Herrero-Climent, M.; Rios-Carrasco, E.; Rios-Santos, J.V.; Pérez, R.A.; Manero, J.M.; Gil Mur, J.; Herrero-Climent, M. Influence of the Elastic Modulus on the Osseointegration of Dental Implants. *Materials* **2019**, *12*, 980. [CrossRef]
50. Li, Y.; Yang, C.; Zhao, H.; Qu, S.; Li, X.; Li, Y. New Developments of Ti-Based Alloys for Biomedical Applications. *Materials* **2014**, *7*, 1709–1800. [CrossRef]

51. Yilmaz, E.; Gökçe, A.; Findik, F.; Gülsoy, H. Powder Metallurgy Processing of Ti-Nb Based Biomedical Alloys. *Acta Phys. Pol. A* **2018**, *134*, 278–280. [CrossRef]
52. Hanada, S.; Masahashi, N.; Semboshi, S.; Jung, T. Low Young's modulus of cold groove-rolled β Ti–Nb–Sn alloys for orthopedic applications. *Mater. Sci. Eng. A* **2021**, *802*, 140645. [CrossRef]
53. Masahashi, N.; Mizukoshi, Y.; Semboshi, S.; Ohtsu, N.; Jung, T.; Hanada, S. Photo-induced characteristics of a Ti–Nb–Sn biometallic alloy with low Young's modulus. *Thin Solid Film.* **2010**, *519*, 276–283. [CrossRef]
54. Aleixo, G.T.; Lopes, E.S.; Contieri, R.; Cremasco, A.; Afonso, C.R.M.; Caram, R. Effects of Cooling Rate and Sn Addition on the Microstructure of Ti-Nb-Sn Alloys. *Solid State Phenom.* **2011**, *172*, 190–195. [CrossRef]
55. Han, M.-K.; Kim, J.-Y.; Hwang, M.-J.; Song, H.-J.; Park, Y.-J. Effect of Nb on the Microstructure, Mechanical Properties, Corrosion Behavior, and Cytotoxicity of Ti-Nb Alloys. *Materials* **2015**, *8*, 5986–6003. [CrossRef]
56. Xu, W.; Lu, X.; Zhang, B.; Liu, C.; Lv, S.; Yang, S.; Qu, X. Effects of Porosity on Mechanical Properties and Corrosion Resistances of PM-Fabricated Porous Ti-10Mo Alloy. *Metals* **2018**, *8*, 188. [CrossRef]
57. Progri, R.; Villechaise, B.; Godet, M. Boundary Conditions in a Two-Body Contact Formed by a Rectangular Polyurethane Slab Pressed Against an Araldite Plane. *J. Tribol.* **1985**, *107*, 138–141. [CrossRef]
58. Johnson, A.W.; Bull, C.W.; Kumar, K.S.; Briant, C.L. The influence of microstructure and strain rate on the compressive deformation behavior of Ti-6Al-4V. *Metall. Mater. Trans. A* **2003**, *34*, 295–306. [CrossRef]
59. Dean, J.; Clyne, T. Extraction of plasticity parameters from a single test using a spherical indenter and FEM modelling. *Mech. Mater.* **2017**, *105*, 112–122. [CrossRef]
60. Rielli, V.V.; Amigó-Borrás, V.; Contieri, R.J. Single step heat treatment for the development of beta titanium composites with in-situ TiB and TiC reinforcement. *Mater. Charact.* **2020**, *163*, 110286. [CrossRef]
61. Schroeder, H.A.; Balassa, J.J. Abnormal trace metals in man: Niobium. *J. Chronic Dis.* **1965**, *18*, 229–241. [CrossRef]
62. Electronic Irish Statute Book (eISB). Available online: http://www.irishstatutebook.ie/eli/1993/si/389/made/en/print (accessed on 23 December 2020).
63. U.S. Food & Drug Administration. Available online: https://www.accessdata.fda.gov/scripts/cdrh/cfdocs/cfcfr/cfrsearch.cfm?fr=73.575 (accessed on 23 December 2020).
64. Rajagopalan, M.; Tschopp, M.A.; Solanki, K.N. Grain Boundary Segregation of Interstitial and Substitutional Impurity Atoms in Alpha-Iron. *JOM* **2014**, *66*, 129–138. [CrossRef]
65. Li, Y.-H.; Rao, G.-B.; Rong, L.-J.; Li, Y.-Y. The influence of porosity on corrosion characteristics of porous NiTi alloy in simulated body fluid. *Mater. Lett.* **2002**, *57*, 448–451. [CrossRef]
66. Prashanth, K.G.; Zhuravleva, K.; Okulov, I.; Calin, M.; Eckert, J.; Gebert, A. Mechanical and Corrosion Behavior of New Generation Ti-45Nb Porous Alloys Implant Devices. *Technologies* **2016**, *4*, 33. [CrossRef]
67. Afzali, P.; Ghomashchi, R.; Oskouei, R.H. On the Corrosion Behaviour of Low Modulus Titanium Alloys for Medical Implant Applications: A Review. *Metals* **2019**, *9*, 878. [CrossRef]
68. Ferro, R.; Saccone, A. *Intermetallic Chemistry*, 1st ed.; Elsevier: Amsterdam, The Netherlands, 2007; pp. 7–80.
69. Gai, X.; Bai, Y.; Li, S.; Wang, L.; Ai, S.; Hao, Y.; Yang, R.; Dai, K. Review on Corrosion Characteristics of Porous Titanium Alloys Fabricated by Additive Manufacturing. *J. Shanghai Jiaotong Univ.* **2021**, *26*, 416–430. [CrossRef]
70. Romero-Resendiz, L.; Gómez-Sáez, P.; Vicente-Escuder, A.; Amigó-Borrás, V. Development of Ti–In alloys by powder metallurgy for application as dental biomaterial. *J. Mater. Res. Technol.* **2021**, *11*, 1719–1729. [CrossRef]
71. Bania, P.J. Beta titanium alloys and their role in the titanium industry. *JOM* **1994**, *46*, 16–19. [CrossRef]
72. Atapour, M.; Pilchak, A.L.; Frankel, G.S.; Williams, J.C. Corrosion Behavior Of β Titanium Alloys For Biomedical Applications. *Mater. Sci. Eng. C-Mater* **2011**, *31*, 885–891. [CrossRef]
73. Codaro, E.; Nakazato, R.; Horovistiz, A.; Ribeiro, L.; Ribeiro, R.; Hein, L. An image analysis study of pit formation on Ti–6Al–4V. *Mater. Sci. Eng. A* **2003**, *341*, 202–210. [CrossRef]
74. Yılmaz, E.; Gökçe, A.; Findik, F.; Gulsoy, H.O.; Iyibilgin, O. Mechanical properties and electrochemical behavior of porous Ti-Nb biomaterials. *J. Mech. Behav. Biomed. Mater.* **2018**, *87*, 59–67. [CrossRef] [PubMed]
75. Fontana, M.G. Corrosion Engineering. In *Corrosion Engineering*, 3rd ed.; McGraw-Hill Book Company: New York, NY, USA, 1986; Volume 6.
76. Eisenbarth, E.; Velten, D.; Müller, M.; Thull, R.; Breme, J. Biocompatibility of β-stabilizing elements of titanium alloys. *Biomaterials* **2004**, *25*, 5705–5713. [CrossRef] [PubMed]